

Hydrothermally grown nanostructured WO_3 films and their electrochromic characteristics

This article has been downloaded from IOPscience. Please scroll down to see the full text article.

2010 J. Phys. D: Appl. Phys. 43 285501

(<http://iopscience.iop.org/0022-3727/43/28/285501>)

View [the table of contents for this issue](#), or go to the [journal homepage](#) for more

Download details:

IP Address: 139.179.96.60

The article was downloaded on 28/09/2010 at 11:30

Please note that [terms and conditions apply](#).

Hydrothermally grown nanostructured WO₃ films and their electrochromic characteristics

Zhihui Jiao¹, Xiao Wei Sun^{1,3}, Jinmin Wang¹, Lin Ke² and Hilmi Volkan Demir¹

¹ School of Electrical and Electronic Engineering, Nanyang Technological University, Nanyang Avenue, Singapore 639798, Singapore

² Institute of Material Research and Engineering, 3 Research Link, Singapore 117602, Singapore

E-mail: exwsun@ntu.edu.sg

Received 18 February 2010, in final form 21 May 2010

Published 28 June 2010

Online at stacks.iop.org/JPhysD/43/285501

Abstract

We report the synthesis of nanostructured tungsten trioxide (WO₃) films and their electrochromic characteristics. Plate-like monoclinic WO₃ nanostructures were grown directly on fluorine-doped tin oxide glass substrates by a simple and low-cost crystal-seed-assisted hydrothermal method. The growth mechanism of the film is investigated. HRTEM analysis reveals the single crystalline quality of the WO₃ nanostructure. The film exhibits tunable transmittance modulation under different voltages and repetitive cycling between the clear and blue states has no deleterious effect on its electrochromic performance after 3000 cycles. The electrochromic device composed of the WO₃ film has high electrochromic stability, colour contrast and reasonable switching response with a colouration efficiency of 38.2 cm² C⁻¹ at 632.8 nm.

(Some figures in this article are in colour only in the electronic version)

1. Introduction

Electrochromic (EC) devices are capable of reversibly changing their optical properties upon charge injection and extraction induced by an external voltage, which makes them suitable for various applications including EC displays [1–4], smart windows [5–9], self-dimming rear mirrors [10] and sensors [11]. As a well-known inorganic EC material, WO₃ can display blue colour and become colourless by alternating the polarity of the applied voltage. It has been extensively studied as an EC material because it exhibits a high colouration efficiency (CE) and a high cyclic stability compared with other transition metal oxides [12–15]. Moreover, WO₃-based EC devices exhibit low power consumption, a good memory effect and a high contrast ratio [16]. Traditionally, WO₃ is assembled as a thin film on a conductive substrate that serves as the working electrode. To date several methods have been used to fabricate WO₃ thin film electrodes including sputtering [17], pulsed laser deposition [18], electrosynthesis [19], sol-gel [20] and hydrothermal method [21]. Generally, vacuum

techniques are expensive and the as-prepared film is denser. For electrosynthesis, a high energy input (high voltage or current) is usually needed. Sol-gel processing following the dip-coating method requires less capital to deposit WO₃ films over large areas with high efficiency. However, particular attention must be paid to the chemistry of solutions and the annealing conditions to get stable and good adhesive WO₃ films with desired microstructures and thicknesses.

In comparison, the hydrothermal approach is promising for fabricating WO₃ film because of its merits of low reaction temperature, flexible substrate selection and easiness in scaling up. Recently, there have been reports on the synthesis of various one-dimensional (1D) WO₃ nanostructures such as nanorods [22] and nanoribbons [23]. However, growing directly a uniform WO₃ nanostructure thin film with good adhesion on a substrate still remains a challenge. Moreover, there are no reports on the studies of the EC characteristics of hydrothermally grown WO₃ films.

In this letter, we present a directly grown nanostructured uniform WO₃ film using the hydrothermal method and its EC characteristics.

³ Author to whom any correspondence should be addressed.

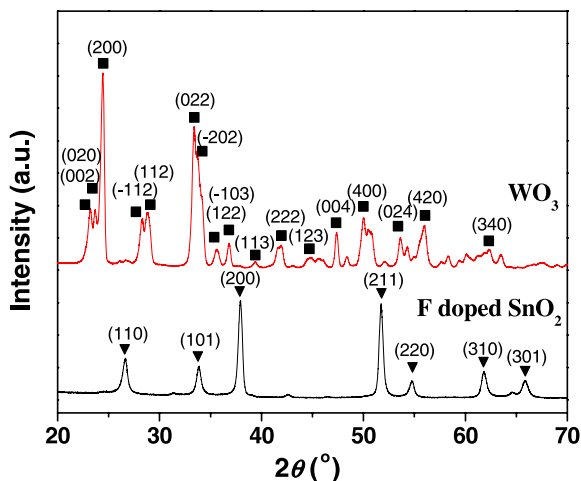


Figure 1. XRD patterns of bare FTO and as-prepared WO_3 thin films.

2. Experimental

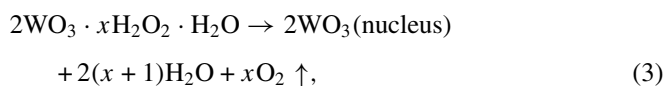
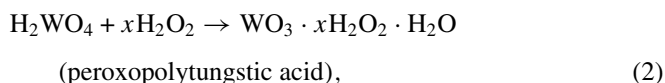
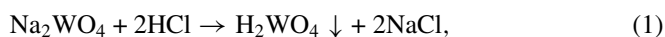
The typical synthesis procedure is described as follows. First, 1 g $\text{Na}_2\text{WO}_4 \cdot 2\text{H}_2\text{O}$ was dissolved in 15 ml de-ionized water, and then HCl solution was added until no more precipitate formed. The precipitate was washed using de-ionized water in an ice bath many times. Then 2 ml H_2O_2 was added into the precipitate under intense stirring and its temperature was raised to obtain a WO_3 seed solution. The mixture was then spin coated onto fluorine-doped tin oxide (FTO) glasses that were previously cleaned by acetone, isopropanol and de-ionized water in sequence. Subsequently, the substrates were heated to 400°C in atmosphere for 40 min. Meanwhile, the as-prepared WO_3 seed solution was diluted using de-ionized water and transferred into an autoclave as the hydrothermal reaction precursor. The prepared FTO glass substrates with a WO_3 seed layer were put into an autoclave for hydrothermal growth where the reaction was maintained at 180°C for 12 h. In comparison, a bare FTO glass substrate was also used as the reference (i.e. the negative control group). The crystal structure of the products was characterized by x-ray powder diffraction (XRD, Siemens) using $\text{Cu K}\alpha$ ($\lambda = 0.15406 \text{ nm}$) radiation. The morphologies of the as-prepared thin films were observed by field-emission scanning electron microscopy (FESEM, JSM-6700F). High-resolution transmission electron microscope (HRTEM) images were obtained using a JEM-2010 microscope with an accelerating voltage of 200 kV. Cyclic voltammetry (CV) of the films was measured by a three-electrode system (VersaSTAT 3F Potentiostat/Galvanostat) with 0.2M lithium perchlorate (LiClO_4) in γ -butyrolactone as the electrolyte, Pt as the counter electrode and Ag/AgCl as the reference electrode. The transmittance spectra were measured by a UV-Vis spectrophotometer (Lambda 950).

3. Results and discussion

Figure 1 shows the XRD patterns of the bare FTO substrate and the as-prepared products grown by the hydrothermal method. The XRD pattern of the substrate can be indexed to F-doped

SnO_2 . For the hydrothermally grown product, different peaks can be seen. All the peaks can be indexed to the monoclinic phase of WO_3 (JCPDS 83-0950) with lattice constants of $a = 7.301 \text{ \AA}$, $b = 7.539 \text{ \AA}$ and $c = 7.690 \text{ \AA}$. The sharp peaks indicate the as-synthesized thin film is of high crystal quality.

The morphologies of the as-synthesized products on bare FTO and seeded FTO substrates are shown in figure 2. It can be seen that sparsely distributed WO_3 particles with a size of $\sim 2 \mu\text{m}$ are present for the reference sample without a seed layer (figure 2(a)). These particles showed weak adhesion to the FTO substrate and could be easily dislodged by the de-ionized water. Moreover, there are numerous empty surface regions without WO_3 growth and hence the coverage uniformity of these aggregated particles is poor. For comparison, using the seed layer coated on the surface of FTO, a uniform WO_3 thin film composed of plate-like nanostructures is grown on the surface (figures 2(b) and (c)). The growth mechanism of the plate-like nanostructured WO_3 film can be explained according to the following reactions:



H_2WO_4 precipitate was formed after HCl solution was added into the Na_2WO_4 solution. Then it was dissolved by adding hydrogen peroxide (H_2O_2) and peroxopolytungstic acid (PTA) was formed. WO_3 crystal nucleus was obtained when the reaction temperature exceeded the decomposition temperature of PTA. With a uniform layer of WO_3 seed layer, the nucleation on the substrate is uniform and uniform plate-like WO_3 nanostructured films can be grown. It can be seen that there are some pores existing between the plates. These pores are formed by stacking of the nanoplates. The calculated porosity of the WO_3 film using the Brunauer-Emmett-Teller (BET) method is about 5.4% with an average pore size of 63.7 nm. The pores between the nanoplates can increase the interface area between WO_3 and electrolyte and reduce the diffusion path length of ions. Porous WO_3 films contributing to fast ion diffusing kinetics can result in better EC performances compared with the solid film [13]. It can be seen from the cross sectional SEM image in the inset of figure 2(c) that the thickness of the as-synthesized film is $\sim 1.5 \mu\text{m}$. Figure 2(d) shows the HRTEM image of a single plate-like WO_3 piece. Clear lattice fringes corresponding to the (200) plane can be identified, indicating the single crystal quality of the WO_3 nanostructure. It is well known that the EC performance of WO_3 is closely related to its level of crystallization [24]. Generally, amorphous WO_3 shows faster EC switching response compared with the crystalline one due to a larger specific surface area [25, 26]. However, the cyclic stability of amorphous WO_3 is poorer compared with the

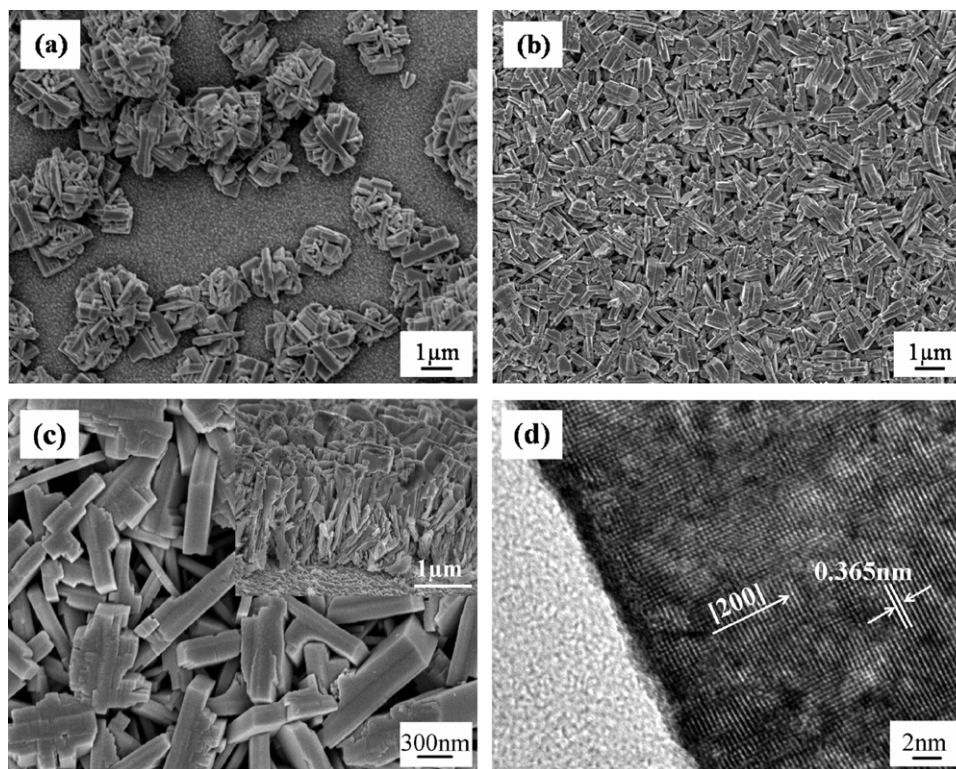
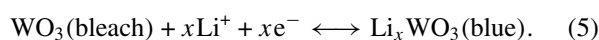


Figure 2. (a) SEM images of WO_3 microparticles grown without a seed layer; (b), (c) as-prepared WO_3 thin film, inset of figure (c) is the cross sectional SEM image; (d) HRTEM image of a single WO_3 plate-like nanostructure.

crystalline WO_3 because of more defect states such as $\text{W}-\text{O}-\text{H}$ and $\text{W}=\text{O}$ sites, which may act as intercalated ion trapping sites [27]. The amorphous WO_3 can only be used in lithium-based electrolytes since its uncompact structure has a high dissolution rate in acidic electrolyte, while the crystalline WO_3 can endure acidic electrolyte without degradation for a long cyclic time. Moreover, EC devices based on crystalline WO_3 can modulate the optical transmission by reflection (particularly in the near infrared region) whereas amorphous WO_3 does that by absorption [28, 29]. For smart window applications where the main purpose is to produce energy-efficient glazing, crystalline WO_3 should have some advantages.

Figure 3 shows the transmittance spectra of the WO_3 film recorded at -1.0 , -2.0 and -3.0 V. With increasing negative bias, the WO_3 EC film gradually changes from semi-transparent colourless to deep blue. The peak transmittance wavelengths measured at -1.0 V, -2.0 V and -3.0 V are 597 nm, 492 nm and 427 nm, respectively, showing an obvious blue-shift.

To investigate the stability of ion intercalation/deintercalation, CV curves were recorded for the 1st and 3000th cycles at room temperature (figure 4). The test was performed at a 100 mV s^{-1} sweep speed between -1.0 and 1.0 V. The recorded current is due to cation intercalation/deintercalation according to the following reaction. During each run, the colour of the film is observed to change from blue to semi-transparent colourless reversibly:



From figure 4, it can be seen that there is no obvious change in the current densities after 3000 cycles, only a slight reduction

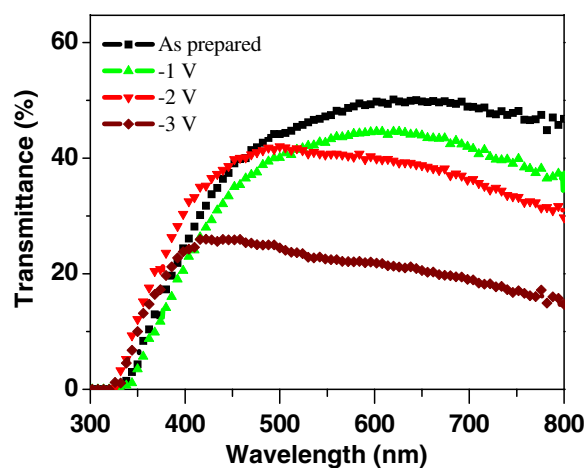


Figure 3. Transmittance spectra of the WO_3 film measured at 0 V, -1.0 V, -2.0 V and -3.0 V.

at the oxidization end is observed. This indicates the high stability of the as-prepared WO_3 film. The CV curves of the WO_3 film recorded between ± 0.8 V at various scan rates from 5 to 100 mV s^{-1} are shown in figure 4(b). As the scan rate is increased, the anodic peaks corresponding to the Li^+ deintercalation gradually shift towards the positive potential. Moreover, the ratio between the cathodic peak current and anodic peak current density is less than unity, which is similar to the spray pyrolysis synthesized WO_3 films [27]. The inset of figure 4(b) shows the cathodic and anodic peak current density values (j_{pa} and j_{pc}) as a function of the square root of the scan rate ($v^{1/2}$). It can be seen that an approximate

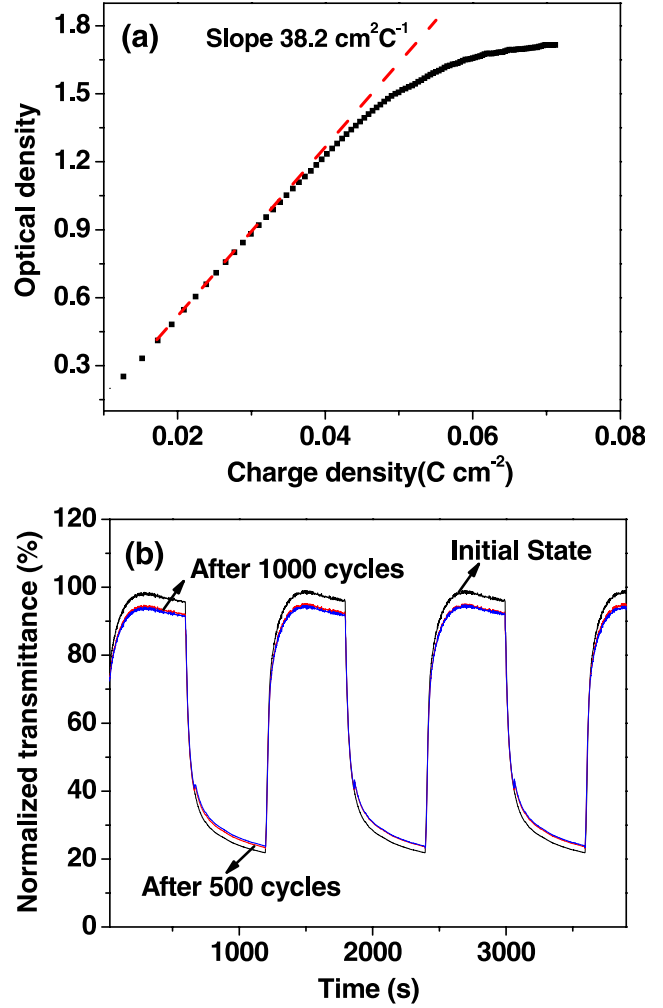
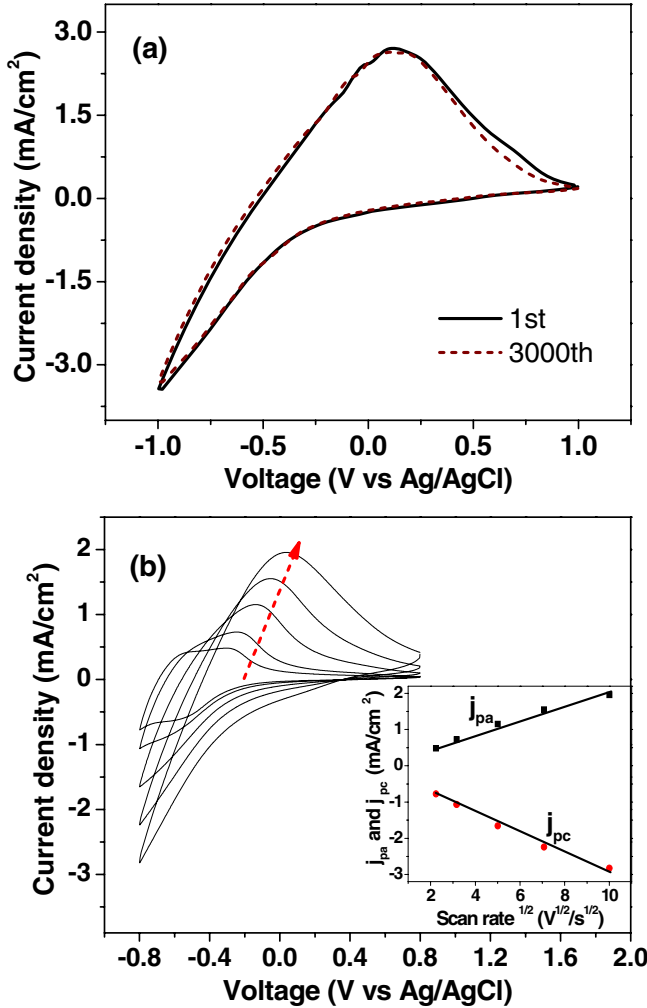


Figure 4. (a) CV curves of the WO₃ thin film at the 1st and 3000th cycle. The measurement was performed in 0.2M LiClO₄/γ-butyrolactone with a sweep rate of 0.1 V s⁻¹. (b) CV curves recorded at 5 mV s⁻¹, 10 mV s⁻¹, 25 mV s⁻¹, 50 mV s⁻¹ and 100 mV s⁻¹, respectively. The inset shows the cathodic/anodic peak current density as a function of the square root of the scan rates.

linear dependence is obtained indicating the cyclic process is diffusion controlled. The effective diffusion coefficient D of Li⁺ ions during intercalation and deintercalation can be calculated from the cathodic and anodic peak current (i_{pc} and i_{pa}) dependence on the square root of the potential scan rate ($v^{1/2}$) assuming a simple solid state diffusion controlled process [30]:

$$\delta i_p / \delta \sqrt{v} = 2.69 \times 10^5 n^{3/2} A C \sqrt{D}, \quad (6)$$

$$D = 0.1382 \times 10^{-10} n^{-3} A^{-2} C^{-2} (\delta i_p / \delta \sqrt{v})^2, \quad (7)$$

where n is the number of electrons transferred in unit reaction, A is the effective geometric surface area of the WO₃ electrode and C is the concentration of the diffusion species (Li⁺). The effective diffusion coefficient D_{Li^+} was calculated from equation (7) to be $2.73 \times 10^{-11} \text{ cm}^2 \text{ s}^{-1}$ and $1.44 \times 10^{-11} \text{ cm}^2 \text{ s}^{-1}$ for the intercalation and deintercalation processes, respectively. The D_{Li^+} values are in quantitative agreement with the data calculated by Bathe and Patil [27]. It

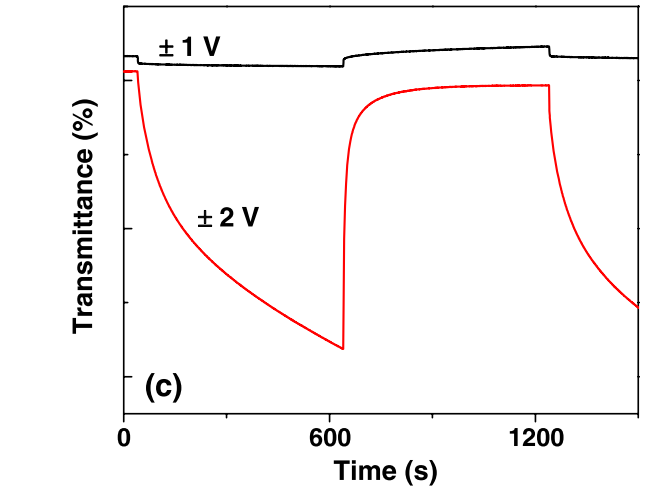


Figure 5. (a) OD variation with respect to the charge density (measured at 632.8 nm, -3 V bias). (b) Switching time characteristics between the coloured and bleached states for EC device measured at ±3 V. (c) Switching time characteristics for the device measured at ±1 V and ±2 V.

is well known that the switching response is largely dependent on the diffusion coefficient of diffusion species, and large diffusion coefficient will result in fast response.

The CE represents the change in the optical density (OD) per unit charge density (Q/A , where Q is the charge

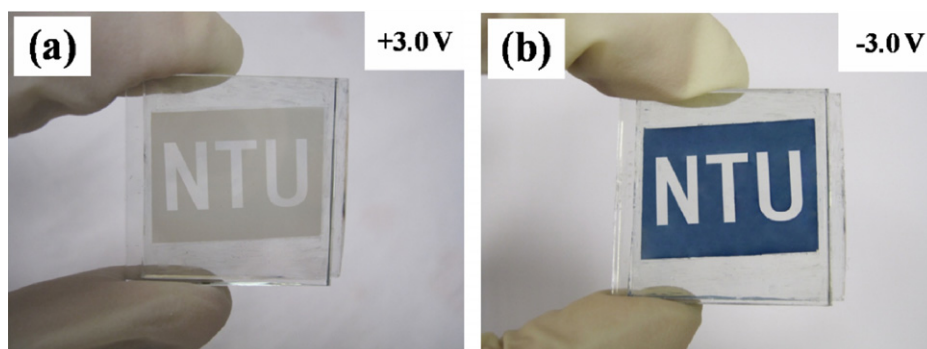


Figure 6. A WO_3 -based EC display after biasing at +3 V (a) and (b) -3 V.

and A is the area) during switching and can be calculated according to the formula $\text{CE} = \Delta\text{OD}/(Q/A)$, where $\Delta\text{OD} = \log(T_{\text{colour}}/T_{\text{bleach}})$. Figure 5(a) shows OD versus the intercalation charge density at -3 V of colouration potential and at a wavelength of 632.8 nm. The CE was extracted as the slope of the line fitted to the linear region of the curve. The calculated CE value is $38.2 \text{ cm}^2 \text{ C}^{-1}$, which is comparable to the other reported crystalline WO_3 structures [31].

A square wave voltage was applied (between -3.0 and 3.0 V) to investigate the transition response time between colouration and bleaching, and colour switching stability. Figure 5(b) shows the dynamic colouration/bleaching characteristics of the EC device composed of WO_3 thin film recorded at a wavelength of 632.8 nm for the 1st, 500th and 1000th cycles. The colouration and bleaching time can be defined as the time required for 50%, 70% and 90% changes in the whole transmittance modulation, respectively. The colouration time of 50% changes $t_{\text{c}(50\%)}$ is found to be 22 s while the bleaching time $t_{\text{b}(50\%)}$ is 23 s. For 70% modulation, $t_{\text{c}(70\%)} = 51 \text{ s}$ and $t_{\text{b}(70\%)} = 36 \text{ s}$, which are comparable to amorphous structures [25]. However, the crystalline WO_3 is stabler than the amorphous one. The switching time further increases to $t_{\text{c}(90\%)} = 236 \text{ s}$ and $t_{\text{b}(90\%)} = 95 \text{ s}$ for 90% modulation. Compared with WO_3 nanorods fabricated by the hydrothermal method and assembled on conductive substrates by dip-coating ($t_{\text{c}(90\%)} = 272 \text{ s}$ and $t_{\text{b}(90\%)} = 364 \text{ s}$) [32], the colouration and bleaching time for 90% modulation is 36 s and 269 s shorter, respectively. Moreover, considering that the as-prepared WO_3 EC film ($\sim 1.5 \mu\text{m}$) is much thicker than the film assembled by dip-coating [32] or the Langmuir-Boldget approach [33], the fast switching time is further appreciated. It is also worth mentioning that there is no observable degradation after 500 cycles in our experiment, which indicates the good switching stability of the WO_3 film. The switching response time for the EC device based on the WO_3 film were also investigated for both ± 1 and $\pm 2 \text{ V}$ switching (figure 5(c)). For $\pm 1 \text{ V}$ switching, the contrast achieved between coloured and bleached states is small. While for $\pm 2 \text{ V}$ switching, the transmittance change increases much more significantly. The obtained responses for 90% transmittance change are $t_{\text{c}(90\%)} = 332 \text{ s}$, $t_{\text{b}(90\%)} = 213 \text{ s}$ for $\pm 1 \text{ V}$ switching, and $t_{\text{c}(90\%)} = 450 \text{ s}$, $t_{\text{b}(90\%)} = 37 \text{ s}$ for $\pm 2 \text{ V}$ switching. The response for colouration at $\pm 1 \text{ V}$ is faster than the one at $\pm 2 \text{ V}$, which is primarily due to shallow level colouration for the small bias voltage.

Figure 6 shows an EC display based on this patterned film with another bare FTO substrate used as the counter electrode. Lithium perchlorate (LiClO_4) in γ -butyrolactone (0.2M) was filled in between the two electrodes as the electrolyte. At biases of $\pm 3 \text{ V}$, a good contrast can be seen for a wide range of viewing angles. The colour can be retained for several hours after removal of the external voltage for our unsealed devices.

4. Conclusions

In summary, uniform WO_3 thin films with plate-like nanostructures on FTO glass substrates were synthesized via a simple low-cost hydrothermal approach. EC display based on this film showed good colouration/bleaching switching characteristics. There is a good prospect of applying these hydrothermal WO_3 thin films in smart windows and electronic papers.

References

- [1] Schoot C J, Ponjee J J, Van-Dam H T, Van-Doorn R A and Bolwijn P T 1973 *Appl. Phys. Lett.* **23** 64
- [2] Yamanaka K 1987 *J. Appl. Phys.* **26** 1884
- [3] Bonhôte P, Gogniat E, Campus F, Walder L and Grätzel M 1999 *Displays* **20** 137
- [4] Wang M J, Fang G J, Yuan L Y, Huang H H, Sun Z H, Liu N H, Xia S H and Zhao X Z 2009 *Nanotechnology* **20** 185304
- [5] Lampert C M 1994 *Sol. Energy Mater. Sol. Cells* **32** 307
- [6] Rauh R D 1999 *Electrochim. Acta* **44** 3165
- [7] Kraft A and Rottmann M 2009 *Sol. Energy Mater. Sol. Cells* **93** 2088
- [8] Granqvist C G 1994 *Renew. Energy* **5** 141
- [9] Yoshimura H and Koshida N 2006 *Appl. Phys. Lett.* **88** 093509
- [10] Bange K and Gambke T 1990 *Adv. Mater.* **2** 10
- [11] Cantalini C, Sun H T, Faccio M, Pelio M, Santucci S, Lozzi L and Passacantando M 1996 *Sensors Actuators B: Chem.* **31** 81
- [12] Vidotti M and De-Torresi S I C 2008 *J. Braz. Chem. Soc.* **19** 1248
- [13] Deepa M, Srivastava A K, Sood K N and Agnihotry S A 2006 *Nanotechnology* **17** 2625
- [14] Nishio K, Iwata K and Masuda H 2003 *Electrochim. Solid-State Lett.* **6** H21
- [15] Lee S H, Cheong H M, Tracy C E, Mascarenhas A, Czanderna A W and Deb S K 1999 *Appl. Phys. Lett.* **75** 1541
- [16] Nah Y C, Ghicov A, Kim D and Schmuki P 2008 *Electrochim. Commun.* **10** 1777
- [17] Miller E L, Marsen B, Cole B and Lum M 2006 *Electrochim. Solid State Lett.* **9** G248

- [18] Kawasaki H, Namba J, Iwatsuji K, Suda Y, Wada K, Ebihara K and Ohshima T 2002 *Appl. Surf. Sci.* **197** 547
- [19] Liao C C, Chen F R and Kai J J 2007 *Sol. Energy Mater. Sol. Cells* **91** 1282
- [20] Cheng W, Baudrin E, Dunn B and Zink J I 2001 *J. Mater. Chem.* **11** 92
- [21] Wang J M, Lee P S and Ma J 2009 *Cryst. Growth Des.* **9** 2293
- [22] Wang J M, Khoo E, Lee P S and Ma J 2009 *J. Phys. Chem. C* **113** 9655
- [23] Gu Z J, Zhai T Y, Gao B F, Sheng X H, Wang Y B, Fu H B, Ma Y and Yao J N 2006 *J. Phys. Chem. B* **110** 23829
- [24] Agrawal A, Cronin J P and Zhang R 1993 *Sol. Energy Mater. Sol. Cells* **31** 9
- [25] Deepa M, Joshi A G, Srivastava A K, Shivaprasad S M and Agnihotry S A 2006 *J. Electrochem. Soc.* **153** C365
- [26] Subrahmanyam A and Karuppasamy A 2007 *Sol. Energy Mater. Sol. Cells* **91** 266
- [27] Bathe S R and Patil P S 2009 *Smart Mater. Struct.* **18** 025004
- [28] Cogan S F, Plante T D, Parker M A and Rauh R D 1986 *Sol. Energy Mater. Sol. Cells* **14** 185
- [29] Svensson, J S E M and Granqvist C G 1985 *Thin Solid Films* **126** 31
- [30] Shiyanovskaya I and Hepel M 2000 *J. New Mater. Electrochem. Syst.* **3** 241
- [31] Lee S H, Deshpande R, Parilla P A, Jones K M, To B, Mahan A H and Dillon A C 2006 *Adv. Mater.* **18** 763
- [32] Wang J M, Khoo E, Lee P S and Ma J 2008 *J. Phys. Chem. C* **112** 14306
- [33] Yoo S J, Lim J W and Sung Y E 2007 *Appl. Phys. Lett.* **90** 173126